



Centrifuge observations on multidirectional loading of a suction caisson in dense sand

L. Zhao^{1,2} · M. F. Bransby² · C. Gaudin²

Received: 7 September 2019 / Accepted: 10 April 2020 / Published online: 29 April 2020
© Springer-Verlag GmbH Germany, part of Springer Nature 2020

Abstract

This paper presents centrifuge tests undertaken to investigate the combined VH capacities of suction caisson in sand under multidirectional loadings following series of low magnitude horizontal cyclic loading. These loading paths are relevant to foundations of array of floating renewables such as wave energy converters or wind turbines. The centrifuge tests mainly provide information about the $V-H$ yield envelopes in different loading directions and the H_x-H_y yield envelopes in the horizontal plane so that the effect of multidirectional loading can be analysed. The evolution of the yield envelope after cyclic loadings is first presented. Yield envelopes for load change angle β of 60° , 90° , 120° from the initial horizontal cyclic loading direction are then presented, and the mechanisms for increased capacity for $\beta > 90^\circ$ and reduced capacity for $\beta < 90^\circ$ are discussed.

Keywords Centrifuge modelling · Multidirectional loadings · Offshore renewables · Sand · Suction caisson · Yield envelope

1 Introduction

Future developments in offshore renewable energy generation are likely to involve the use of floating structures such as wind turbines and wave energy converters (WEC) in deeper waters. These are likely to be installed in ‘farms’ or arrays of multiple devices in order to be commercially viable [6, 9]. The traditional mooring solution for a single floating structure is to have three or four anchors (or anchor clusters) each connected to the device via one mooring line [28]. This results in the anchor loaded in a single horizontal direction. Using this strategy would require large numbers

of anchors (e.g. 3 N or 4 N anchors (or anchor clusters), where N is the number of floating devices) and consequently large anchoring/mooring system costs. An alternative mooring approach is to use shared anchors so that each anchor supports several mooring lines, each orientated at an angle β to each other (see Fig. 1a). This reduces the number of anchors significantly (from 300 to approximately 100 for an array of 100 floating devices as depicted in Fig. 1a, see [12] and offers the potential for considerable costs savings. However, such mooring configurations require anchors to be designed against loading that comes from multiple directions and that are cyclic in nature.

One possible anchoring solution is the suction caisson anchor. This is a circular foundation (of diameter D) with a skirt around the periphery (of skirt length L), which is usually installed by ‘suction’ by reducing the pressure inside of the caisson forcing the skirts into the seabed. Once installed, the caisson anchor acts like a short rigid pile and is capable of resisting vertical, lateral and moment loads.

Estimation of the capacity of caisson anchors under combined loads is usually based on the methods of limit equilibrium [1] or plastic limit analysis [5, 20], and the maximum holding capacity is obtained if the mooring line

✉ L. Zhao
liang.zhao.geotechnical@gmail.com

M. F. Bransby
fraser.bransby@uwa.edu.au

C. Gaudin
christophe.gaudin@uwa.edu.au

¹ Present Address: Fugro GeoConsulting, 58 Mounts Bay Road, Perth, WA 6000, Australia

² Centre for Offshore Foundation Systems, Oceans Graduate School, University of Western Australia, 35 Stirling Hwy, Crawley, Perth, WA 6009, Australia

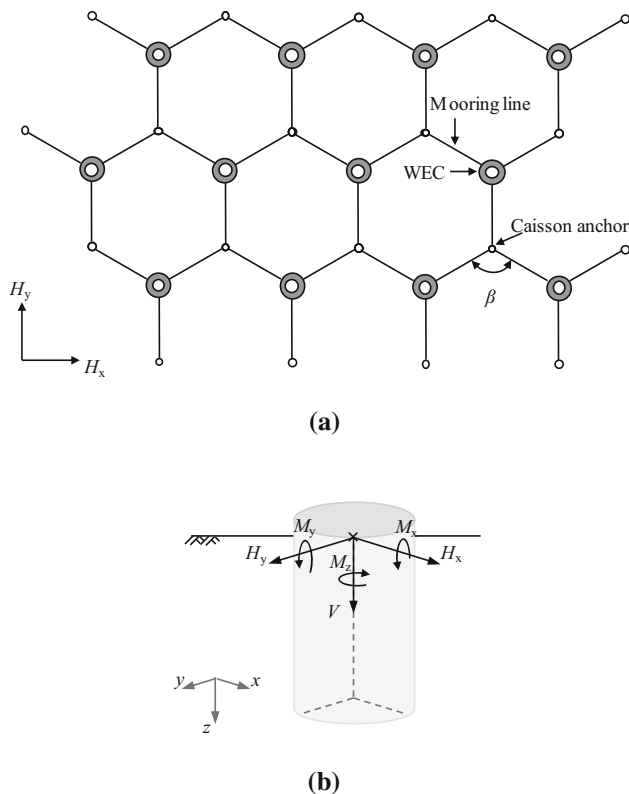


Fig. 1 Shared caisson anchor for offshore floating renewables, **a** example of array of wave energy converters and multidirectional loaded caisson, **b** general loading conditions for shared caisson anchor

is attached at the optimal load depth where a translational failure mode is achieved. However, existing knowledge and guidelines (e.g. [2–4]) are mostly for caissons under unidirectional loadings and there is limited understanding of how such anchors or foundations would respond when the loading direction changes (e.g. [30]). The majority of studies on the effect of multidirectional loading are focused on pile foundations and the development of Winkler-type models (e.g. [17, 19, 24]), where the pile–soil interaction mechanisms away from the soil surface along the pile may be quite different to those occurring during loading of a low aspect ratio caisson foundation or anchor.

This paper focuses on the capacities of a caisson in drained medium dense sand under multidirectional loading. In particular, the variation of caisson capacity when loaded successively in different directions (with angle between loading directions, $\beta = 0^\circ, 60^\circ, 90^\circ, 120^\circ$ in the horizontal plane) after cyclic loading in a single direction ($\beta = 0^\circ$) is investigated in the geotechnical centrifuge. The objective is to characterise yield envelopes in the vertical (V)–horizontal (H) load space that can assist in the design of foundations under multidirectional loading.

2 Multidirectional loading on caisson in sand

The capacity of a caisson under combined loading is commonly estimated by creating an interaction diagram in load space defining an envelope of load combinations (a ‘yield envelope’) where failure (or plastic deformation) occurs. Loads are normally assumed to act within a plane, so the envelope is defined in vertical (V), horizontal (H) and moment (M) load space (e.g. [8, 16, 27]). However, the general loading conditions include the six possible three-dimensional load components V, H_x, H_y, M_x, M_y and M_z (with the axis defined in Fig. 1b). In either case, the size of the yield envelope is generally defined by the vertical caisson capacity (governed by the vertical plastic penetration, e.g. Gottardi et al. [14]).

Before a foundation has experienced any horizontal or moment load (in spatially uniform soil conditions on a flat seabed), the horizontal capacity will be independent of the direction of the horizontal load (in the H_x – H_y plane) due to the axi-symmetry of both the caisson geometry and the soil state around the caisson. Consequently, H_x – H_y cross sections of the general six-dimensional yield envelope at any fixed vertical load will be circular, and the capacity of the caisson for any in-plane loading (in whichever x – y direction) can be described with a single planar (V – H – M) yield envelope.

However, as soon as non-vertical loads are applied to a foundation, for example, a horizontal loading in the x direction (H_x) or a moment about the x -axis (M_x), these loadings will introduce changes in the stress field and/or density field in the soil around the caisson, which is no longer axi-symmetric. Consequently, the subsequent foundation capacity in different directions will differ (e.g. the horizontal capacity in the x -direction will differ to that in the y -direction and the envelope H_x – H_y cross sections will no longer be circular). Therefore, to use the yield envelope approach, the evolving (six-dimensional) shape of the V – H_x – H_y – M_x – M_y – M_z yield envelope will need to be understood.

This paper explores how cross sections of the yield envelope (with no caisson rotation) vary when the caisson is subjected first to cyclic loading in one horizontal direction. Experiments were performed in a geotechnical centrifuge, whereby an initial horizontal cyclic loading was applied to the caisson and the subsequent capacity of the caisson was explored by investigating V – H yield envelope cross sections for different x – y plane loading directions (with a load change angle β in the H_x – H_y plane as shown in Fig. 1a). The results are also combined to investigate H_x – H_y cross sections at fixed vertical loads.

3 Experimental equipment

3.1 The 4D ‘robot’

Centrifuge tests were performed in the 10 m diameter 240 g-tonne centrifuge at the University of Western Australia [13] at a centrifuge acceleration of 19.17 g with the rotation radius measured at the tip of the caisson. The set-up used a four degree-of-freedom actuator, the 4D ‘robot’, enabling (1) in-flight (i.e. without stopping the centrifuge) repositioning of the model caisson between consecutive tests and (2) measurements of horizontal load in the direction of the loading by rotating the loading leg used to measure horizontal loadings. The leg was bolted to the tool holder of the ‘robot’ through a ‘sleeve’ with high bending stiffness, as shown in Fig. 2a. The bending gauges on the loading leg work only in the direction they are facing, shown as the positive y -axis direction in Fig. 2a, b. Consequently, out-of-plane loadings were applied to the foundation by rotating the ‘robot’ arm to the targeted direction of the loading plane. A rotation adapter is connected to the caisson foundation, shown in Fig. 2, such that the caisson remains still and the surrounding soil undisturbed while the loading leg is rotated with the robot. The horizontal load (H) was derived from the difference in bending moment recorded by two independent bending gauges (gauge A and B shown in Fig. 2b) with known distance between the gauges, while the axial load (V) was measured directly by an axial load cell located between the

bending leg and the rotation adapter (see Fig. 2). The very slight flexing of the loading leg (required to generate a signal for measurement of bending strain) led to a maximum deformation of the loading arm of 0.80 mm (at model scale). In the tests, vertical load (V) was zeroed at the initial penetration depth (z) before each test, but a correction had to be made for the change in uplift force induced by the change in caisson submerged weight as the caisson was penetrated into the water. This was achieved by correcting the load measured by the force generated by the volume of water displaced during penetration.

Displacement control in directions x , y , z and rotation (β) was achieved by the hydraulic powered ‘robot’, and load control was performed in all the directions via a software feedback loop.

3.2 Model caisson

The model caisson used in the centrifuge tests has an aspect ratio of $L/D = 0.5$ and two drainage holes in the caisson top cap, which were used to drain the water freely in the tests. The tests did not aim at replicating specific prototypes conditions, but rather at investigating in very well controlled conditions the multidirectional capacity of caisson in sand. Accordingly, the caisson dimensions were relatively small with length $L = 19$ mm and diameter $D = 38$ mm ($L = 0.364$ m and $D = 0.728$ m at prototype scale at the tested g -level), shown in Table 1. The dimensions were limited by the capacities of the bending gauges and to avoid significant elastic bending deformation from

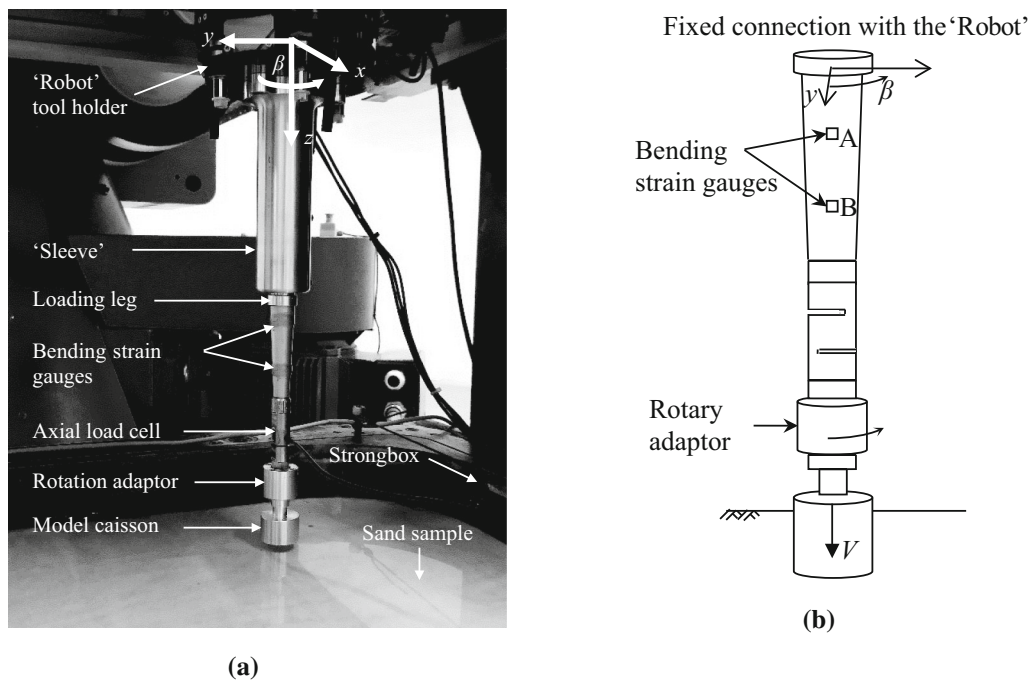


Fig. 2 Test set-up, **a** 4D ‘robot’ and test set-up in the centrifuge, **b** schematic diagram of ‘Robot’ rotation

Table 1 Caisson and soil properties

Parameters		Values
Caisson (prototype scale)	Caisson outside diameter, D	0.728 m
	Caisson skirt length, L	0.364 m
	Caisson skirt thickness, t	0.02 m
Superfine silica sand	Specific gravity, G_s	2.67
	Minimum void ratio, e_{\min}	0.49
	Maximum void ratio, e_{\max}	0.78
	Effective unit weight, γ'	$\sim 10.46 \text{ kN/m}^3$
	Relative density, D_r	$\sim 50\%$

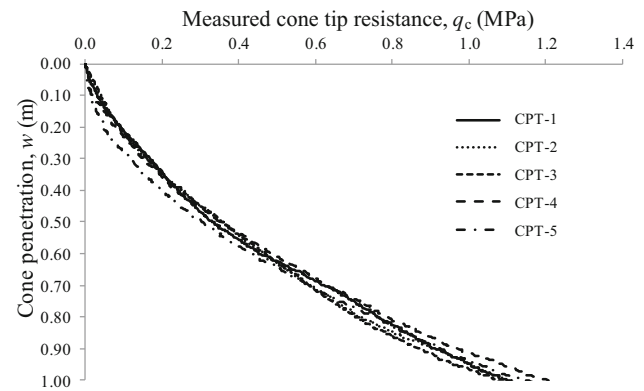
the bending leg due to the lateral soil resistance. However, the selected model foundations size allowed multiple tests to be conducted in a single (20 m by 20 m prototype plan dimension) sand sample, which increased test repeatability and allowed sufficient tests to be conducted to investigate the effect of load direction changes.

3.2.1 The sand sample

Tests were performed in water saturated sand. The sand used in the centrifuge tests is a commercial superfine silica sand supplied by Sibelco Australia. It has been routinely used at UWA for many years, and its basic properties are summarised in Table 1. More details can be found in Liu and Lehane [18] and Chow et al. [10]. It is noted that the ratio of wall thickness to particle size (t/D_{50}) is small (~ 5.6). However, Tran et al. [26] revealed that this ratio had only a small influence on the pure vertical capacity. Consequently, the effect of t/D_{50} is presumed to be insignificant especially for the inclined loading caisson conditions investigated herein.

The sand sample was prepared in a large strongbox, of internal dimensions $1 \text{ m} \times 1 \text{ m} \times 0.5 \text{ m}$ (width \times length \times depth), by dry pluviation to achieve a medium dense state by controlling drop height and flow rate. Saturation of the sand sample was achieved by infiltrating water from the base of the strong box to approximately 20 mm above the soil surface.

Cone penetration tests (CPTs) were carried out with a cone of diameter 7 mm at different locations in the sand sample to investigate the uniformity of the sand sample, and the results show good consistency (see Fig. 3). The sand sample has an average saturated unit weight of 10.46 kN/m^3 resulting in a relative density $D_r \approx 50\%$.

**Fig. 3** Results of CPTs

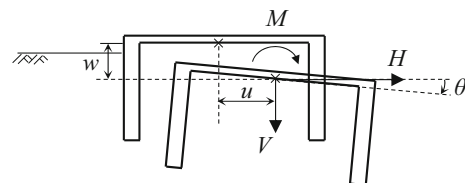
4 Test programme

The V – H yield envelope cross sections were tracked using sideswipe tests [25]: moving the foundation horizontally at a fixed vertical position. No caisson rotation during the sideswipe tests was permitted. Consequently, the load paths generate moment loading, rather than following a true ($M = 0$) cross section through the yield envelope. Due to the likely associated flow observed for loadings in the H – M plane [27], this will lead to probing a V – H path where the maximum H is mobilised for the given vertical load [29].

Sign conventions and notations for loads and displacement are shown in Fig. 4 as defined by Butterfield et al. [7], and the reference point (RP) was taken as the centre base of the top plate. Prototype units will be used in the presentation of the results in this paper unless otherwise specified.

The following test procedure was used

1. The caisson was first installed by vertical penetration of the foundation into the soil sample at a constant rate of 0.05 mm/s until a vertical load of $V_{\text{install}} = 36.8 \text{ kN}$ was achieved (load path OA shown in Fig. 5a). The value of 36.8 kN was selected as the load required to ensure that the skirts were fully embedded, and the top plate was in contact with the sand surface. The penetration of the caisson skirt-tip into the soil, w_{install} , was constant for all the tests, and the ratio to the caisson skirt length, w_{install}/L , is about 0.98, as shown in Table 2.

**Fig. 4** Caisson geometry and sign conventions (for in-plane loading)

2. After installation, the caisson was continuously pushed vertically under displacement control until a maximum vertical load, $V_{0i} = 184.1$ kN, was achieved (path AB in Fig. 5a). V_{0i} is the same for all the tests (except OM-07) to ensure that the caisson (plastic) penetration is the same and the resulting initial yield envelopes are comparable.
3. For the monotonic tests, the foundation was brought to a target initial vertical load, V_i (which could either equal V_{0i} or approximately zero load). Then, the sideswipes were carried out, shown as the path BC with tests starting at $V_i = V_{0i}$ and as $B'C'$ for tests starting near-zero ($V_i \approx 0$ kN) in Fig. 5a. By using two different starting values of V_i at $V_i = 0$ and $V_i = V_{0i}$, the test programme enables sideswipe tests to track the V – H yield envelope from both ‘ends’ (Fig. 5a).
4. For the multidirectional tests, lateral cyclic loading was firstly applied in the direction H_x shown in Fig. 5b. Then, the loading direction was rotated by an angle β ($= 0^\circ, 60^\circ, 90^\circ, 120^\circ$) with respect to H_x . Finally, the yield envelopes were investigated by performing step 2 and 3 in the new load direction.

All 17 tests were carried out in one sample in the strongbox with sufficient test spacing ($> 4D$) to minimise boundary and interaction effects, which also minimises the errors caused by potential sand density variations between samples. The displacement rate during all loading stages was set at of 0.01 mm/s (at model scale), so drained soil

behaviour was generated. The tests are grouped according to their types with details summarised in Table 2.

5 Test results: in-plane loading

5.1 Pure vertical loading

Results from the initial vertical loading stages are summarised in Fig. 6. The data sets start after the initial installation (involving penetration of the skirts into the soil and then the top cap of the caisson coming into contact with the seabed) which involved applying a vertical load, $V_{install}$ of 36.8 kN where the displacement, w , was zeroed. The graphs show subsequent vertical loading until 184.1 kN was applied (except in test OM-07 where 221 kN was applied).

The vertical loading response was used to define a plastic hardening law (relationship between vertical capacity and vertical penetration) for the purpose of correcting the yield envelop from two sources of errors in sideswipe tests [14]: (1) the elastic deformation of the loading leg and (2) elastic vertical displacement recovery of the soil.

An elastic stiffness, $k_e = 78,000$ kN/m was measured (in Fig. 6) and used to relate change of load (ΔV) to change in elastic caisson penetration (Δw_e):

$$\Delta w_e = \Delta V / k_e \tag{1}$$

Then, the vertical load (V) can be expressed using Eq. 2 considering the amount of plastic penetration (w_p) and elastic penetration (w_e) occurring:

$$V = V_{install} + \frac{k_e k_p}{k_e - k_p} w_p \tag{2}$$

where the caisson vertical loading stiffness, $k_p = 2900$ kN/m. The resulting fit to the data is shown in Fig. 6.

5.2 Deduced V – H yield envelope for initial loading

The V – H yield envelope for the caisson without any prior H or M load history was investigated by carrying out sideswipe tests in a single direction (H_x shown in Fig. 5b) directly after installation. Two tests were undertaken following the procedure detailed in the previous section to establish the yield envelope from both ‘ends’. The resulting yield envelope is used as a benchmark for later comparison and is expected to be isotropic (i.e. independent of the direction of horizontal loading in the H_x – H_y plane).

The resulting V – H load paths from the two sideswipe tests are shown in Fig. 7a. The load path from high initial vertical load (OM-09) demonstrates a typical parabolic

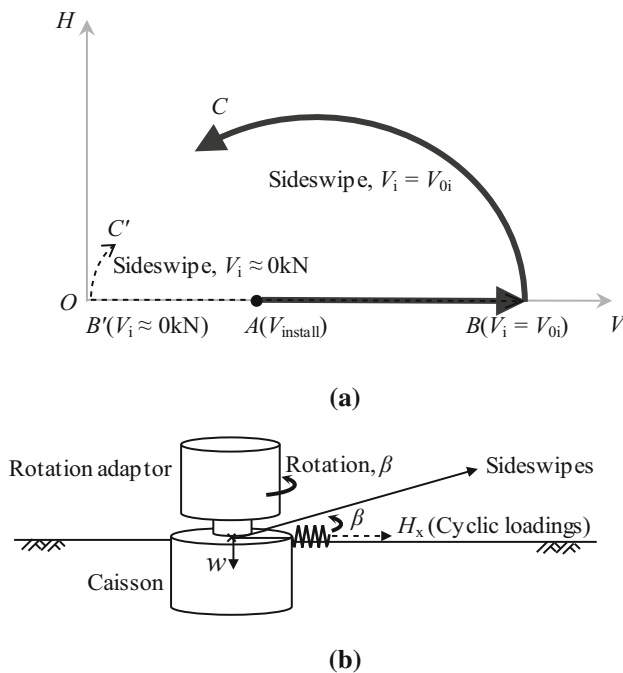
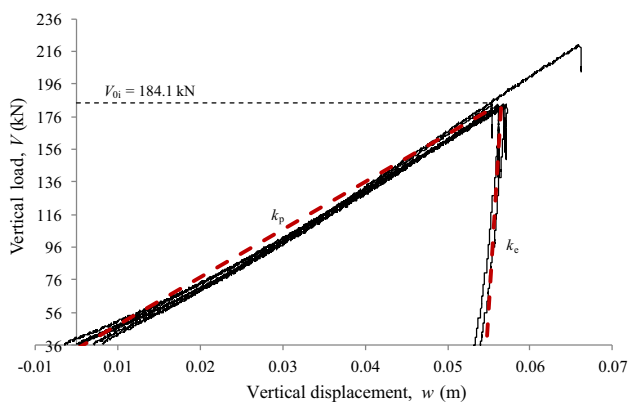


Fig. 5 Tests strategies, a the load paths, b multidirectional loadings

Table 2 Tests design and results summary

Test group	Sub-group	Test reference	Rotation β ($^{\circ}$)	Installation embedment w_{install}/L (-)	Initial embedment w_i/D (-)	Number of cycles, N (-)	Reference vertical load, V_{0i} (kN)	
Vertical loading	Up to $V = 220.95$ kN	OM-07	–	–	–	–	–	
	Up to $V = 184.13$ kN	OM-05, OM-08, OM-09, OM-10, OC-0-1, OC-0-2, OC-0-3, OC-0-4, OC-0-5, OC-0-6, OC-60-1, OC-60-2, OC-90-1, OC-90-2, OC-120-1, OC-120-2						
Side swipes	From $V = 220.95$ kN	OM-07	0	0.98	1.06	–	220.95	
	From $V = 184.13$ kN	OM-05	0	0.97	1.04	–	184.13	
		OM-09	0	0.97	1.03	–		
		OC-0-1	0	0.99	1.06	10		
		OC-0-3	0	0.97	1.05	60		
		OC-0-5	0	0.97	1.05	30		
		OC-60-1	60	0.97	1.03	30		
		OC-90-1	90	0.98	1.06	30		
		OC-120-1	120	0.97	1.06	30		
		From $V \approx 0$ kN after $V = 184.13$ kN	OM-08	0	0.97	1.01	–	
			OM-10	0	0.98	1.04	–	
			OC-0-2	0	0.99	1.03	10	
			OC-0-4	0	0.96	1.00	60	
			OC-0-6	0	0.96	1.03	30	
			OC-60-2	60	0.98	1.05	30	
			OC-90-2	90	0.99	1.04	30	
OC-120-2	120	0.98	1.04	30				

**Fig. 6** Caisson vertical responses

shape (although there is an initial vertical load reduction due to the creep relaxation of the sand, which occurred before driving the caisson horizontally [15, 25]). The load path from low initial load tracks the low V ‘end’ of the yield envelope and the ‘sliding line’ at large displacement which was also observed from 1 g investigations by Zhao et al. [29].

The load paths shown in Fig. 7a do not represent exactly the shape of the yield envelope, because an amount of caisson plastic penetration occurs due to soil elastic recovery and loading leg series of centrifuge tests on suction caisson elasticity as V decreases at a fixed penetration. Corrections were made accordingly for both effects, and the horizontal and vertical loads are normalised by the vertical capacity, V_0 , calculated using the hardening law

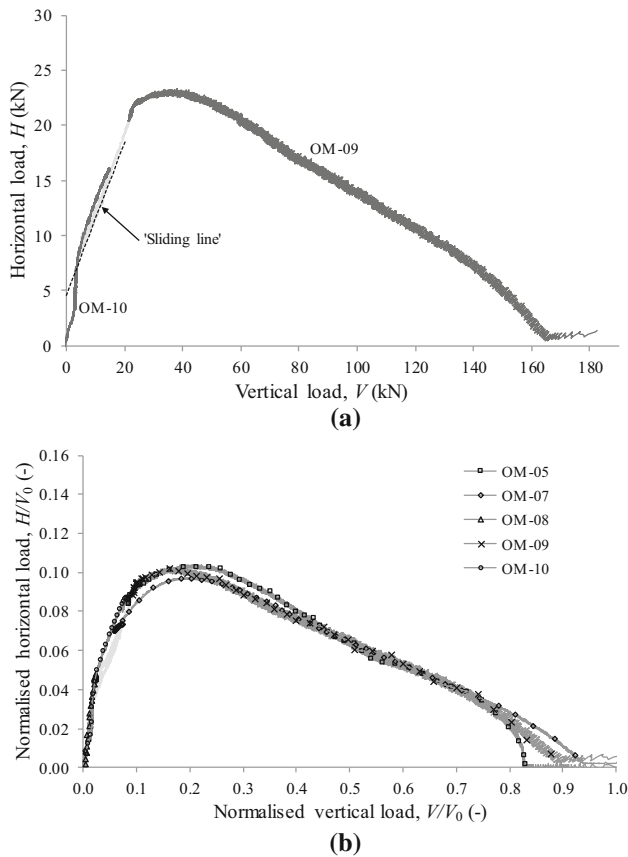


Fig. 7 Yield envelope estimated from sideswipe test for monotonic loading tests, **a** typical sideswipe test results (OM-09 and OM-10), **b** load paths normalised by vertical capacity (V_0)

defined by k_e and k_p . The data from all sideswipe tests have been corrected in the same way in the following analysis.

All the results from sideswipe tests which were conducted immediately after installation are summarised in Fig. 7b, in the dimensionless form of V/V_0 and H/V_0 . These curves show the yield envelope shape for the caisson when first loaded horizontally.

5.3 Unidirectional cyclic loading and in-plane V – H yield envelope hardening

To investigate changes in the in-plane yield envelope as a result of cyclic loading in the same plane, the caisson was first pushed vertically until V_{0i} ($= 184.1$ kN) was reached, then lateral cyclic loading was applied in the x -direction (shown in Fig. 5b) with constant vertical penetration, before the yield envelope was investigated by sideswipe tests conducted in the same loading plane (i.e. with $\beta = 0^\circ$ shown in Fig. 5b).

To allow comparisons between tests, the same constant amplitude lateral cyclic loading was applied, but the number of cycles (N) was varied ($N = 10, 30$ or 60). The

cyclic loading was one-way, with the peak load for each cycle $H_{\max} = 12$ kN about half of the maximum horizontal load observed in the monotonic test shown in Fig. 7a, and the minimum load per cycle, $H_{\min} = 1.8$ kN (see Fig. 8a). The cyclic load period was 20 s (at model scale) to ensure drained conditions.

The V – H load path followed in the cyclic part of the test with 60 cycles (OC-0-3) is shown in Fig. 8b and is compared with the sideswipe results for the tests without cyclic loading (OM-09 and OM-10). The observed load path shown in Fig. 8b is mostly within the original yield envelope estimated from tests OM-09 and OM-10. The vertical load gradually decreases with numbers of cycles until reaching a value of about 5 kN after about 30 cycles, where the load reduces much more slowly per cycle, and where the load path on loading appears to correspond closely to the yield envelope defined by sideswipe test OM-10.

The horizontal load–displacement behaviour during cycling (for OC-0-3) is shown in Fig. 8a, which allows definition of the secant stiffness for each cycle (k_s) and the accumulated lateral displacement u_{ac} at the end of each cycle (corrected from the elastic deformation of the loading arm). The corresponding accumulated horizontal displacement of test OC-0-3 is shown against cycle number in Fig. 8c. Significant horizontal plastic displacement is accumulated (Fig. 8c). Two distinct types of behaviour are observed with a marked increase rate of displacement accumulation (in linear-log scale) observed after about 30 cycles, implying a change of mechanism. Similar changes of response are observed at $N = 30$ for loading stiffness (k_s) versus number of cycles relationship (plotted on Fig. 8d) whereby k_s appears not to change after 30 cycles. The initial reduction in k_s with increasing N is mainly attributed to the decrease in the vertical loading, which could potentially be masking stiffness changes associated with soil densification.

The change in cyclic behaviour after 30 cycles appears to correspond to the load path reaching the low vertical load section of the initial envelope. The increased horizontal displacement accumulation may be associated with either generating a partial sliding ‘failure’ of the soil wedge and base shear or an increased amount of grain migration (as associated with cyclic ratcheting for monopiles, e.g. [11, 21]).

The normalised load path data from the sideswipe tests conducted after the cyclic loading are plotted on Fig. 9, along with the yield envelope for the caisson without previous cyclic loading for comparison. The sideswipe tests starting at large vertical load show that the yield envelope expands with number of cycles for $N = 0$ (the ‘monotonic’ test) to $N = 10$ to $N = 30$. However, the load path for $N = 60$ cuts within the $N = 30$ load path for large

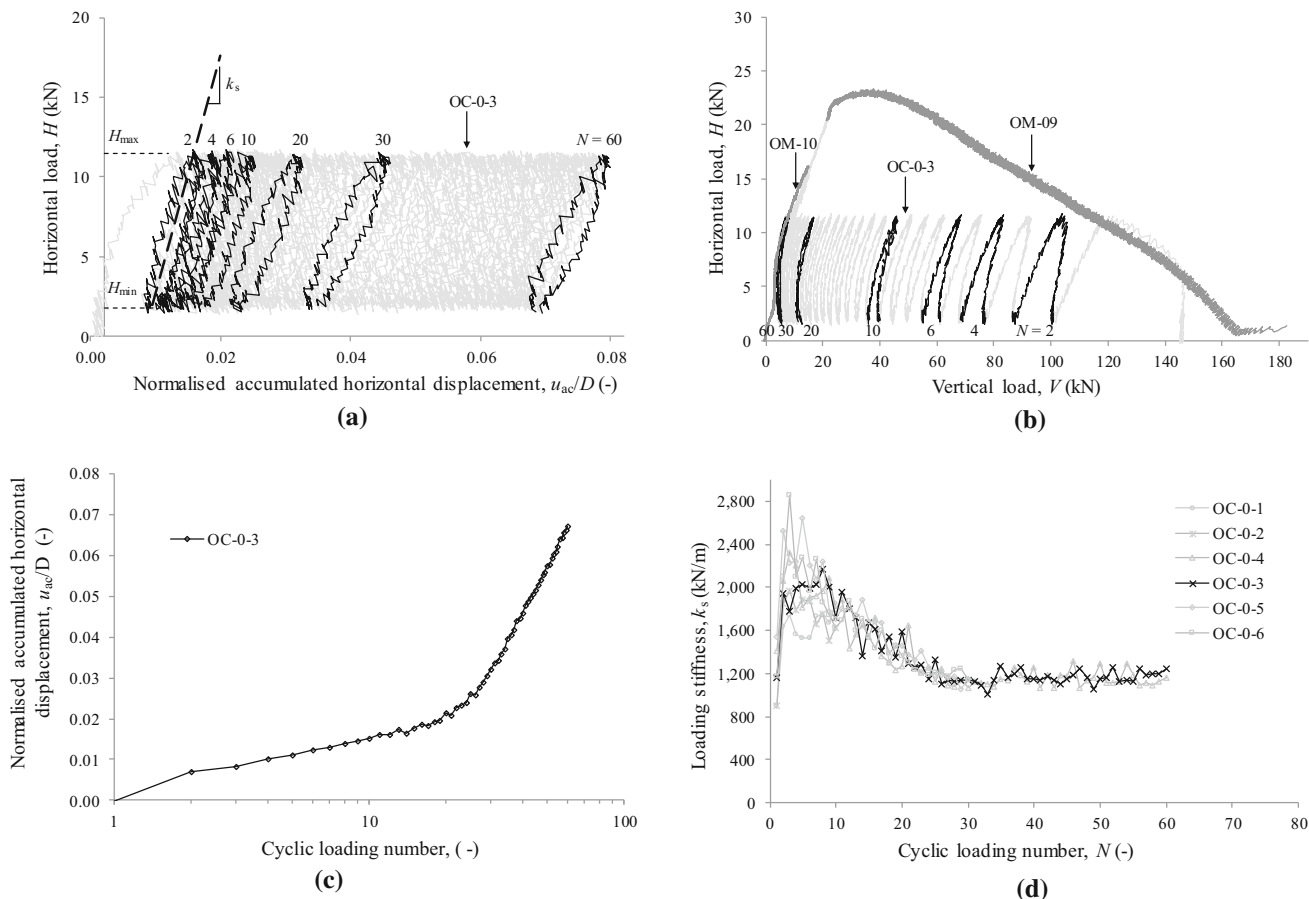


Fig. 8 Typical results of caisson cyclic loadings, **a** load–displacement behaviour (OC-0-3), **b** load path in H – V space, **c** caisson accumulated lateral displacement, **d** Variation of loading stiffness, k_s , with cycle number

V , though appears identical for $V/V_0 < 0.3$. In contrast, all the load paths from sideswipe tests seem to converge to the same ‘sliding line’ [29] at large horizontal displacement, shown as the solid grey lines in Fig. 9.

Figure 10 shows how the horizontal and vertical loads change with horizontal displacement at the beginning of the sideswipe tests with $V_i \approx 0$ kN. Increasing the number of cycles up to $N = 30$ produces an increasing initial horizontal stiffness and quicker mobilisation of vertical load, V . In contrast, the horizontal stiffness and the rate of vertical load mobilisation are lower for the $N = 60$ case compared to the $N = 30$ test.

It can be reasonably assumed that the horizontal load, H , is influenced by two mechanisms during the sideswipe test, lateral soil pressure on the caisson skirt wall and base shearing under zero vertical height change conditions [29]. The different initial stiffness of H in the sideswipe tests can be attributed to one or more of the following mechanisms: (1) increasing sand density in front of the caisson from the cyclic loading leading to increased passive resistance on the skirt wall; (2) increasing sand density at the level of the

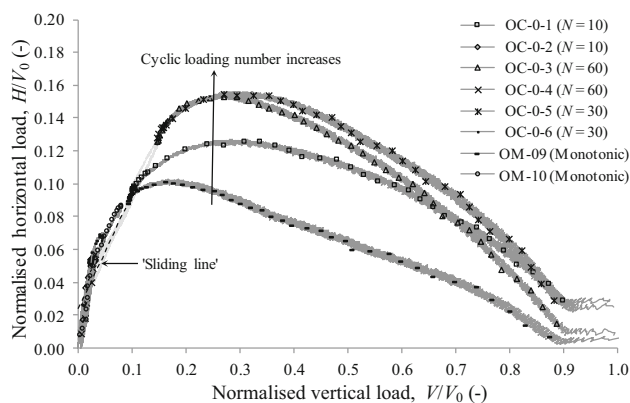
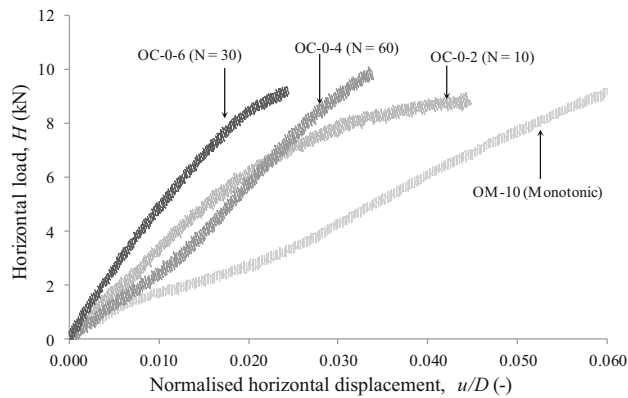
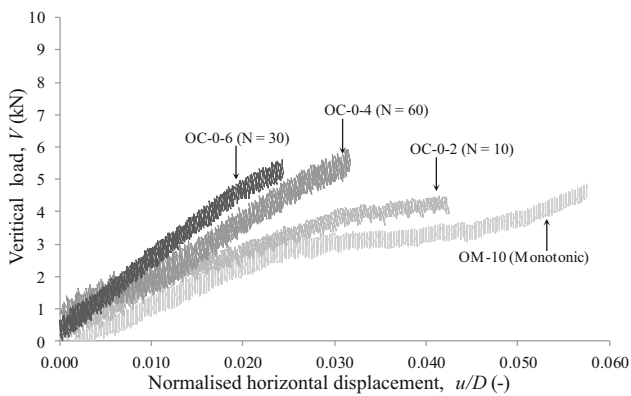


Fig. 9 V – H load paths for sideswipes after different unidirectional cyclic loading events

skirt tips from the cyclic loading leading to stiffer soil and more dilatancy (which also lead to faster increases in V with displacement for the CNS shearing conditions [22] at the foundation base); (3) the generation of a passive soil



(a)



(b)

Fig. 10 The initial sideswipe stiffness for in-plane tests ($V_i \approx 0\text{ kN}$) following the unidirectional cyclic loading: **a** lateral displacement (u/D) versus horizontal load (H), **b** lateral displacement (u/D) versus vertical load (V)

‘berm’ ahead of the caisson due to the accumulated lateral displacement. The changes of soil are schematically illustrated in Table 3 accordingly, and further investigation is required to validate the contributions of these different mechanisms.

6 Test results: multidirectional loading

The test procedure to establish yield envelope for multidirectional loading is similar to that for unidirectional loading. The differences are (1) 30 cycles of loading were applied (in direction H_x) for all tests, and (2) sideswipe tests were carried out in a second horizontal direction at an angle $\beta = 60^\circ, 90^\circ$ and 120° to the original loading direction (see Fig. 6b) thereby exploring a secondary $V-H$ cross section rotated at an angle β to the original plane of loading. As previously, two separate tests were conducted for each condition to explore the yield envelope at both low and large vertical loads.

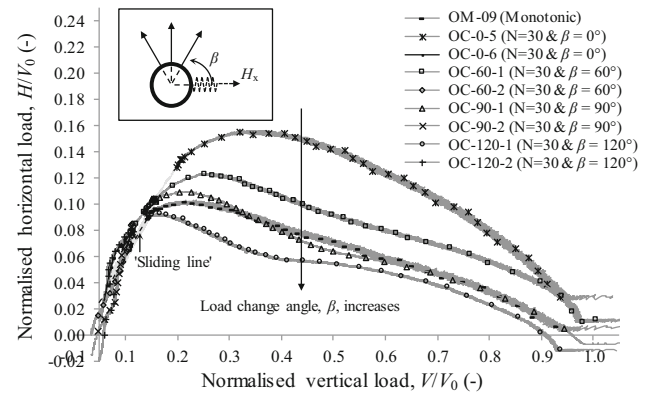


Fig. 11 Estimated yield envelopes for different load directions after cyclic unidirectional loading

For the cyclic (in-plane) stage of each test, an average lateral displacement, $u_{ac}/D \approx 0.025$, was recorded after completion of the cyclic loading sequence, and there were no visible variations of the soil surface around the caisson from video observations during testing. Consequently, the caisson effective embedment, acknowledging that caisson penetration is constant during sideswipe tests, can be assumed to be the same for all the tests. This is an important consideration when discussing changes in horizontal resistance.

Figure 11 summarises the load paths from the sideswipe tests with load change angles of β ($0^\circ, 60^\circ, 90^\circ$ and 120°) and also shows the sideswipe results without cyclic loading (test OM-09, ‘monotonic’). Generally, the size of the yield envelope reduces as the load change angle, β , increases. The same data are also replotted in Fig. 12 to show deduced cross sections in H_x-H_y space at three vertical loads ($V/V_0 = 0.2, 0.3$ and 0.5) from the different sideswipe tests to show how the caisson capacity varies for different loading directions as a result of the initial cyclic loading. Figure 12 shows the data both normalised by the vertical capacity, H/V_0 (in Fig. 12a) and by the horizontal capacity in the original (x -) direction at the same vertical load, H/H_{0v} (in Fig. 12b).

Both Figs. 11 and 12 indicate that the cyclic loading (1) increases foundation capacity (at least for $V/V_0 > 0.15$) when the load direction angle $\beta < 90^\circ$, and (2) ‘softens’ the capacity for $\beta > 90^\circ$, and (3) is similar when displaced perpendicularly to the original loading (i.e. $\beta = 90^\circ$). More tests are required to ascertain the generalisability of these observations, particularly for different V/V_0 values. However, as for the unidirectional test results, all load paths from the multidirectional sideswipe tests conducted appear to converge to the same ‘sliding line’, where the sand around the caisson is expected to have reached critical state at large horizontal displacements.

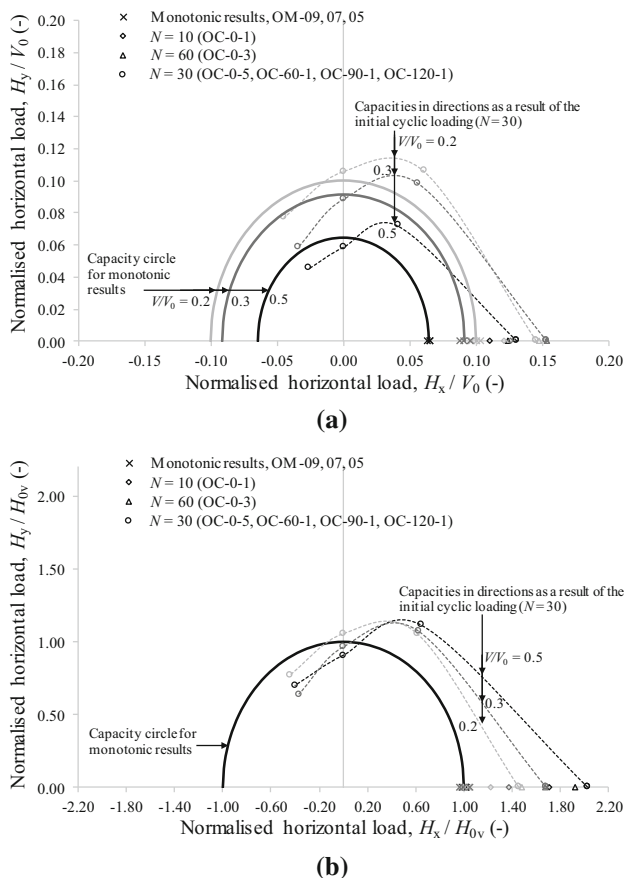


Fig. 12 Failure envelope cross sections in H_x – H_y space from the sideswipe tests at different loading directions, **a** Normalised by V_0 , **b** Normalised by the horizontal capacity at the same vertical load, H_{0v} without any initial cyclic loading

Another way of understanding the asymmetric conditions around the caisson as a result of the in-plane cyclic loading is to examine the initial load–displacement response (as done in the previous section) from the sideswipes starting at low vertical load ($V_i \approx 0$ kN). Figure 13a summarises the initial horizontal load–horizontal displacement behaviour with the corresponding variation of the vertical load, V , summarised in Fig. 13b. The initial stiffness of H in the sideswipe tests decreases noticeably as the load change angle, β , increases, with the stiffness of the $\beta = 90^\circ$ case being about the same as for the foundation without cyclic loading. In contrast, the rate of change of the vertical load with horizontal displacement for different directions is quite similar (except for when $u/D < 0.01$, which is mainly caused by the offset of the initial vertical load before the sideswipe tests) with this rate of change being larger for all loading directions compared to the test without cyclic loading.

The difference of the initial stiffness of the H – u/D relationship shown in Fig. 13a is believed to be mainly due

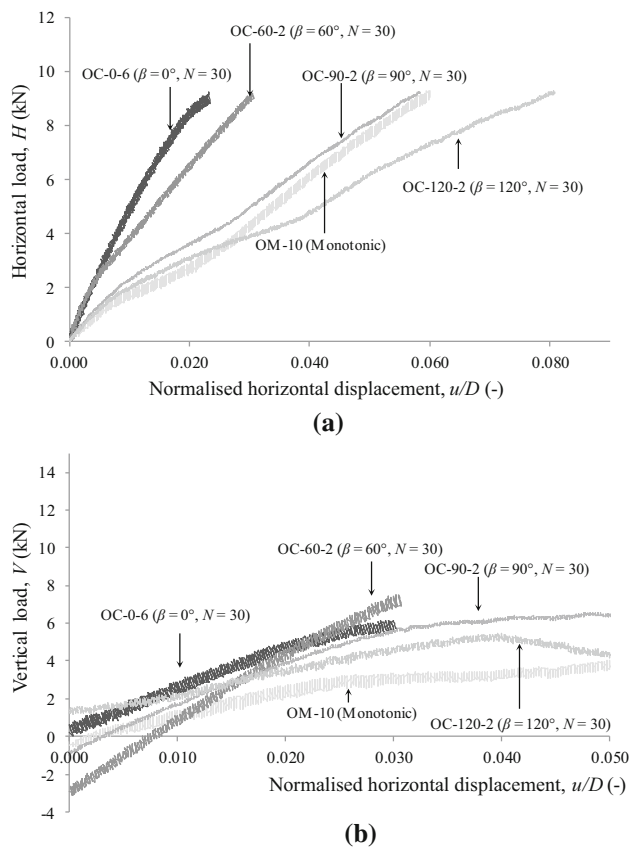


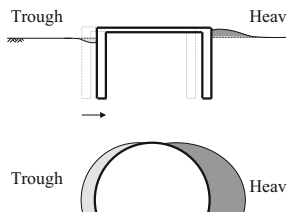
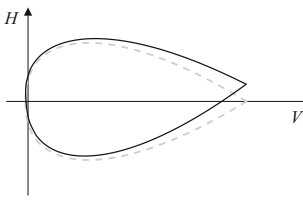
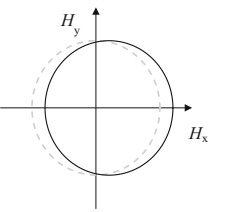

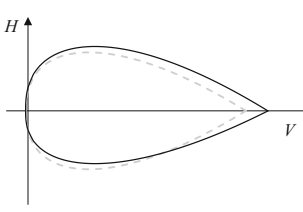
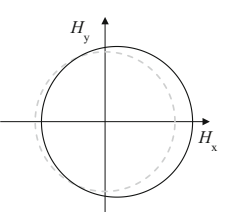
Fig. 13 The initial sideswipe stiffness for multidirectional tests ($V_i \approx 0$ kN) following the unidirectional cyclic loading: **a** lateral displacement (u/D) versus horizontal load (H), **b** lateral displacement (u/D) versus vertical load (V)

to decreasing passive soil resistance on the caisson skirt wall for larger load change angles, due, most likely, to a zone of increased density ‘ahead’ of the caisson (in the x -direction) as a result of the cyclic loading, which becomes less involved in the soil deformation mechanism as the load change angle, β , increases. The small change in the vertical response whatever the loading direction (and the fact that this is larger than for the sideswipe without cyclic loading) suggests that this behaviour is mostly governed by density changes beneath the caisson, because density changes are likely to affect the base dilation response independent of shearing direction.

7 Discussion

The above results have allowed quantification for the first time of the change in V – H_x – H_y capacity (or how the V – H cross section of the six-dimensional yield envelope varies for different load change angles β) for a caisson in medium dense sand subjected to a ‘packet’ of in-plane,

Table 3 Schematic of potential mechanisms

Mechanism	Schematic of changes	Expected effect on in-plane V – H envelope	Expected effect on H_x – H_y cross section
Geometry change only—no volume change			
Asymmetric densification with base densification			

one-way drained cyclic horizontal loading. The envelope appeared to be ‘hardened’ significantly for in-plane loading ($\beta = 0^\circ$) with reducing amount of hardening observed with increasing load change angle so that the capacity is reduced when $\beta > 90^\circ$. Examination of the load–displacement relationships for the initial part of the sideswipe tests conducted from $V_i \approx 0$ kN appear to suggest that there is a zone of denser sand both below and in front (in the original loading direction) of the caisson.

Some potential changes due to in-plane cyclic loading are shown schematically in Table 3 together with how they are expected to change the in-plane V – H yield envelope and the H_x – H_y cross section. For the characteristics of the particular cyclic loading conducted here (with $N = 30$), accumulated cyclic lateral foundation displacements are small ($u_{ac}/D \approx 0.025$) and so geometrical changes (shown in the top row) are likely to be limited. In contrast, changes in soil density in a zone in front, behind and beneath the caisson are likely and are consistent with the changes in yield envelopes and initial loading stiffness and vertical load change trends observed in the tests.

More generally, the type of changes to the density state of the soil around the caisson will depend on the amplitude and duration of cyclic loading and the nature of any geometrical changes around the caisson will depend on both the amount of volume change occurring and, more directly, the amount of accumulated cyclic displacement. It is possible that the $N = 60$ case investigated here (albeit only for in-plane loading) showed less hardening than for the $N = 30$ case because of generating plastic displacement which caused dilation and thereby softening of the soil in

front of and beneath the caisson, although this effect may have been offset by a small amount of soil heave in front of the caisson.

Although this study has only investigated one cyclic loading condition, one sand density state and one caisson geometry, it has revealed that there are range of mechanisms occurring spatially around the caisson which will lead to asymmetry of the 6D yield envelope. Further experimental and/or numerical work is required to elucidate these mechanisms in more detail in order to generate new design approaches to account for the multidirectional loading that will be experienced by anchors for future floating renewable energy farms.

8 Concluding comments

Results of a series of centrifuge tests on suction caisson in sand under multidirectional loadings have been presented. The tests are designed to establish and compare the combined VH capacity with load change angle β of 60° , 90° and 120° from an initial horizontal cyclic loading. The following was observed:

1. Cyclic loading results in a subsequent increased combined capacity in the same vertical plane most likely due to an increase in sand density in front of the caisson (resulting in a higher passive resistance) and at the level of the skirt tips (leading to stiffer soil and more dilatancy). This is valid for a small number of cycles ($N < 30$), after which the accumulation of

horizontal displacement generates a partial sliding ‘failure’ of the soil wedge and base shear or an increased amount of grain migration, resulting in a reduction in the combined capacity (compared to that at $N = 30$).

2. The combined capacity in a vertical plane different to that where horizontal cyclic loading was applied is higher at 60° , identical at 90° and lower at 120° . These changes in horizontal capacity are essentially due to changes in sand density around the caisson, with the zone of increased density in front of the caisson resulting from cyclic loading become less involved in subsequent loading as the direction of load change increases. The change in vertical capacity is limited and independent of the loading direction as it is essentially due to volume change at the base of the caisson, which is largely independent of the shearing direction.

These results present the first observations of the effect of change in loading direction on caisson foundation capacity. Further tests and analyses are required to validate the observations presented and quantify more systematically the change in vertical and horizontal capacity for a broader range of load paths.

Funding Funding was provided by Australian Research Council Discovery Project programme (Grant No. DP150102449).

References

1. Andersen KH (2015) Cyclic soil parameters for offshore foundation design. In: *Frontiers in offshore geotechnics III*, pp 5–82
2. Andersen KH, Murff JD, Randolph MF, Clukey EC, Erbrich CT, Jostad HP, Hansen B, Aubeny C, Sharma P, Supachawarote C (2005) Suction anchors for deepwater applications. In: *The 1st international symposium on frontiers in offshore geotechnics*, ISFOG, Perth, pp 3–30
3. API 2GEO/ISO, 19901-4 (2011) Geotechnical and foundation design considerations, ANSI/API recommended practice. American Petroleum Institute
4. API R (2005) Design and analysis of station keeping systems for floating structures. American Petroleum Institute
5. Aubeny CP, Han SW, Murff JD (2003) Inclined load capacity of suction caissons. *Int J Numer Anal Meth Geomech* 27(14):1235–1254
6. Bakmar CL, Ahle K, Nielsen SA, Ibsen LB (2009) The monopod bucket foundation: recent experiences and challenges ahead. In: *The European offshore wind conference & exhibition*
7. Butterfield R, Houlsby GT, Gottardi G (1997) Standardized sign conventions and notation for generally loaded foundations. *Géotechnique* 47(5):1051–1054
8. Byrne B, Houlsby G, Martin C, Fish P (2002) Suction caisson foundations for offshore wind turbines. *Wind Eng* 26(3):145–155
9. Carter JMF (2007) North Hoyle offshore wind farm: design and build. *Proc Inst Civ Eng Energy* 160(1):21–29
10. Chow SH, Roy A, Herduin M, Heins E, King L, Bienen B, O’Loughlin CD, Gaudin C, Cassidy MJ (2018) Characterisation of UWA superfine silica sand. Centre for Offshore Foundation Systems, Report GEO 18844
11. Cuéllar P, Georgi S, Baeßler M, Rücker W (2012) On the quasi-static granular convective flow and sand densification around pile foundations under cyclic lateral loading. *Granul Matter* 14(1):11–25
12. Fontana CM, Arwade SR, DeGroot DJ, Myers AT, Landon M, Aubeny C (2016) Efficient multiline anchor systems for floating offshore wind turbines. in: *proceedings of the asme 2016 35th international conference on ocean, offshore and arctic engineering*, V006T09A042. ASME, Busan, South Korea
13. Gaudin C, O’Loughlin C, Breen J (2018) A new 240 g-tonne geotechnical centrifuge at the University of Western Australia. In: *Proceedings of the 9th international conference on physical modelling in geotechnics (ICPMG 2018)*, pp 501–506. CRC Press
14. Gottardi G, Govoni L, Butterfield R (2005) Yield loci for shallow foundations by “swipe” testing. In: *Frontiers in offshore geotechnics, ISFOG 2005—proceedings of the 1st international symposium on frontiers in offshore geotechnics*, pp 469–475
15. Govoni L, Gottardi G, Gourvenec S (2010) Centrifuge modelling of circular shallow foundations on sand. *Int J Phys Model Geotech* 10(2):35–46
16. Houlsby GT, Cassidy MJ (2002) A plasticity model for the behaviour of footings on sand under combined loading. *Géotechnique* 52(2):117–129
17. Levy NH, Gaudin C, Einav I (2007) The behaviour of piles undergoing a change in lateral loading direction. *Int J Phys Model Geotech* 7(1):13–23
18. Liu QB, Lehane BM (2012) The influence of particle shape on the (centrifuge) cone penetration test (CPT) end resistance in uniformly graded granular soils. *Géotechnique* 62(11):973–984
19. Mayoral JM, Pestana JM, Seed RB (2005) Determination of multidirectional p - y curves for soft clays. *Geotech Test J* 28(3):253–263
20. Murff JD, Hamilton JM (1993) P-ultimate for undrained analysis of laterally loaded piles. *J Geotech Eng* 119(1):91–107
21. Nicolai G, Ibsen LB, O’Loughlin CD, White DJ (2017) Quantifying the increase in lateral capacity of monopiles in sand due to cyclic loading. *Géotech Lett* 7(3):245–252
22. Ooi L, Carter J (1987) A constant normal stiffness direct shear device for static and cyclic loading. *Geotech Test J* 10(1):3–12
23. Su D, Li JH (2013) Three-dimensional finite element study of a single pile response to multidirectional lateral loadings incorporating the simplified state-dependent dilatancy model. *Comput Geotech* 50:129–142
24. Tan FS (1990) Centrifuge and theoretical modelling of conical footings on sand. Ph.D. Thesis, University of Cambridge
25. Tran MN, Airey DW, Randolph MF (2005) Study of seepage flow and sand plug loosening in installation of suction caissons in sand. In: *The fifteenth international offshore and polar engineering conference*, vol 6. International Society of Offshore and Polar Engineers, Seoul, Korea
26. Villalobos FA, Byrne BW, Houlsby GT (2009) An experimental study of the drained capacity of suction caisson foundations under monotonic loading for offshore applications. *Soils Found* 49(3):477–488
27. Weller SD, Johanning L (2014) Specific requirements for marine renewable energy foundation analysis. In: *Deliverable 4.2 of the DTOcean project*
28. Zhao L, Bransby MF, Gaudin C, Cassidy MJ (2020) Capacity of caissons in dense sand under combined loading. *J Geotech Geoenviron Eng* 146(4):04020009

29. Zhu F, Bienen B, O'Loughlin C, Morgan N, Cassidy MJ (2018) The response of suction caissons to multidirectional lateral cyclic loading in sand over clay. *Ocean Eng* 170(September):43–54

Publisher's Note Springer Nature remains neutral with regard to jurisdictional claims in published maps and institutional affiliations.